Atmos. Chem. Phys. Discuss., doi:10.5194/acp-2015-875, 2016
Manuscript under review for journal Atmos. Chem. Phys.
Published: 22 February 2016

Atmospheric Chemistry and Physics
Discussions
Open Access

Impact of Siberian observations on the optimization of surface CO_2 flux

Jinwoong Kim[1], Hyun Mee Kim[1], Chun-Ho Cho[2], Kyung-On Boo[2], Andrew R. Jacobson[3, 4], Motoki Sasakawa[5], Toshinobu Machida[5], Mikhail Arshinov[6], and Nikolay Fedoseev[7]

[1]{Department of Atmospheric Sciences, Yonsei University, Seoul, Republic of Korea}

[2]{National Institute of Meteorological Research, Jeju, Republic of Korea}

[3]{Earth System Research Laboratory, National Oceanic and Atmospheric Administration, Boulder, USA}

[4]{Cooperative Institute for Research in Environmental Sciences, University of Colorado, Boulder, USA}

[5]{Center for Global Environmental Research, National Institute for Environment Studies, Tsukuba, Japan}

[6]{V. E. Zuev Institute of Atmospheric Optics, Russian Academy of Sciences, Tomsk, Russia}

[7]{Melnikov Permafrost Institute, Russian Academy of Sciences, Yakutsk, Russia}

Correspondence to: Hyun Mee Kim (khm@yonsei.ac.kr)

Abstract

To investigate the effect of additional CO_2 observations in the Siberia region on the Asian and global surface CO_2 flux analyses, two experiments using different observation dataset were performed. One experiment was conducted using a data set that includes additional observations of Siberian tower measurements (Japan-Russia Siberian Tall Tower Inland Observation Network: JR-STATION), and the other experiment was conducted using a data set without the above additional observations. The results show that the global balance of the sources and sinks of surface CO_2 fluxes was maintained for both experiments with and without the additional observations. While the magnitude of the optimized surface CO_2 flux

Atmos. Chem. Phys. Discuss., doi:10.5194/acp-2015-875, 2016
Manuscript under review for journal Atmos. Chem. Phys.
Published: 22 February 2016

Atmospheric Chemistry and Physics Discussions
Open Access

uptake in Siberia decreased, the magnitude of the optimized surface CO_2 flux uptake in the other regions (e.g., Europe) of the Northern Hemisphere (NH) increased for the experiment with the additional observations. This change was mostly caused by changes in the magnitudes of surface CO_2 flux in June and July. The observation impact measured by uncertainty reduction and self-sensitivity tests shows that additional observations provide useful information on the estimated surface CO_2 flux. It is expected that the Siberian observations play an important role in estimating surface CO_2 flux in the NH in the future.

1 Introduction

The terrestrial ecosystem in the Northern Hemisphere (NH) plays an important role in the global carbon balance (Hayes et al., 2011; Le Quéré et al., 2015). Especially, Siberia is considered to be the one of the largest CO_2 uptake regions and reservoirs due to its forest area (Schuleze et al., 1999; Houghton et al., 2007; Tarnocai et al., 2009; Kurganova et al., 2010; Schepaschenko et al., 2011); and its dynamics and interactions with the climate have global significance (Quegan et al., 2011). Therefore, it is important to accurately estimate the surface CO_2 fluxes in this region.

To estimate the surface CO_2 flux, atmospheric CO_2 inversion studies are conducted using atmospheric transport models and atmospheric CO_2 observations (Gurney et al., 2002; Peylin et al., 2013). However, large uncertainties remain in the estimated surface CO_2 fluxes due to the sparseness of current surface CO_2 measurements assimilated by inverse models (Peters et al., 2010; Bruhwiler et al., 2011). Peylin et al. (2013) performed an intercomparison study of estimated surface CO_2 fluxes from 11 different inversion systems. The results showed that the estimated surface CO_2 flux uptake in the NH, where the atmospheric CO_2 network is dense, is similar across the inversion systems; meanwhile, the established flux is noticeably different across the inversion systems for the tropics and SH, where the atmospheric CO_2 network is sparse.

Regionally, however, the longitudinal breakdown of all the NH sinks appears to be much more variable than the total flux itself. Therefore, additional observations in a sparse CO_2 observation network region are necessary to reduce uncertainty in estimating the surface CO_2 flux. Maksyutov et al. (2003) showed that additional observations in the Asia region show the largest effect and reduce the uncertainty in the estimated regional CO_2 fluxes for Siberia during 1992-1996 by time-independent synthesis inversion. Chevallier et al. (2010) also argued that an extension of the observation network toward Eastern Europe and Siberia is necessary to reduce uncertainty in estimated fluxes by inversion methods. Despite the necessity of additional observations in this region, only a few atmospheric CO_2 inversion studies have been conducted using observations in this region due to the deficiency of observations (Quegan et al., 2011).

Meanwhile, Reuter et al. (2014) and Feng et al. (2015) reported that the European terrestrial CO_2 uptake inferred by the satellite-retrieved dry-air column-average model fraction of CO_2 (XCO_2) is larger than that inferred by a bottom-up inventory approach or inverse modeling systems using surface-based in situ CO_2 atmospheric concentrations. Though a broad spatial coverage of XCO_2 from satellite radiance observations provides useful information for inversion systems, the current XCO_2 has low accuracy and regional biases of a few tenths of a ppm, which may hamper the accuracy of estimated surface CO_2 fluxes (Miller et al., 2007; Chevallier et al., 2007). Therefore, in situ observations determined by surface measurements in remote regions are necessary to more accurately estimate the surface CO_2 flux in the inverse models.

To supply additional observations over Siberia to inverse modeling studies, several efforts to observe the atmospheric CO_2 concentrations in Siberia have been conducted. For example, the Max Plank Institute (MPI) operates a tower (since April 2009), accompanied by aircraft measurements (from 1998 to 2005 with 12 to 21 day intervals) at Zotino (ZOTTO; 60.75°N, 89.38°E) (Lloyd et al., 2002; Winderlich et al. 2010). In addition, the Airborne Extensive Regional Observations in Siberia (YAK-AEROBO) aircraft campaign in 2006 (Paris et al., 2008) and Trans-Siberian Observation Into the Chemistry of the Atmosphere (TROICA) project (Turnbull et al., 2009) have measured CO_2 and other chemical species. However these data collected during specific seasons or over only a few years do not provide the long-term CO_2 concentration data necessary to be used as a constraint in the inverse modeling system.

The Center for Global Environmental Research (CGER) of the National Institute for Environmental Studies (NIES) of Japan with the cooperation of the Russian Academy of Science (RAS) constructed a tower network called the Japan-Russia Siberian Tall Tower Inland Observation Network (JR-STATION) in 2002 to measure the continuous CO_2 and CH_4 concentrations (eight towers in central Siberia and one tower in eastern Siberia) and measure the vertical profile of CO_2 from the planetary boundary layer (PBL) to the lower free troposphere by aircraft at one site (Sasakawa et al., 2010; 2013). Saeki et al. (2013) estimated

Atmos. Chem. Phys. Discuss., doi:10.5194/acp-2015-875, 2016
Manuscript under review for journal Atmos. Chem. Phys.
Published: 22 February 2016

Atmospheric Chemistry and Physics Discussions

the monthly surface CO_2 flux for 68 subcontinental regions by using the fixed-lag Kalman smoother and NIES-TM transport model with JR-STATION data. They reported that the inclusion of additional Siberian observation data has an impact on the inversion results showing larger interannual variability over northeastern Europe as well as Siberia, and reduces the uncertainty of surface CO_2 uptake.

CarbonTracker, developed by the National Oceanic and Atmospheric Administration Earth System Research Laboratory (NOAA ESRL) (Peters et al., 2007), is an atmospheric CO_2 inverse modeling system that estimates optimized weekly surface CO_2 flux on a 1°×1° horizontal resolution by using the Ensemble Kalman Filter (EnKF). Since the original CarbonTracker release (Peters et al 2007), a series of improvements have been made with subsequent releases. These include increasing the sites from which CO_2 data are assimilated, increasing the resolution of atmospheric transport, improving the simulation of atmospheric convection in TM5, and the use of multiple first-guess flux models to estimate dependence on priors. These improvements are documented at http://carbontracker.noaa.gov. Several studies have focused on Asia using CarbonTracker (Kim et al., 2012; 2014a; 2014b, Zhang et al., 2014a, 2014b). Schneising et al. (2011) showed that SCanning Imaging Absorption spectroMeter for Atmospheric CHartographY (SCIAMACHY) retrieval data indicate a stronger North American boreal forest uptake and weaker Russian boreal forest uptake compared to CarbonTracker within their uncertainties. On the other hand, Zhang et al. (2014b) estimated surface CO_2 fluxes in Asia by assimilating CONTRAIL (Machida et al., 2008) aircraft CO_2 measurements into the CarbonTracker framework. The results show that surface CO_2 uptake over the Eurasian Boreal (EB) region slightly increases. However, the surface measurements data over the EB region are still not used in the study by Zhang et al. (2014b). Kim et al. (2014b) showed that comprehensive coverage of additional observations in an observation sparse region, e.g., Siberia, is necessary to estimate the surface CO_2 flux in these areas as accurately as that obtained for North America in the CarbonTracker framework using an influence matrix calculation.

In this study, the impact of additional Siberian observations on the optimized surface CO_2 flux over the globe and Asian region within CarbonTracker (The version of CarbonTracker used in this study is based on the CarbonTracker 2010 release) are investigated by comparing the results of estimated surface CO_2 fluxes from two experiments with and without Siberian observations. Section 2 presents the methodology including a priori flux data, atmospheric

CO_2 observations, and experimental framework. Section 3 presents the results, and Section 4 provides a summary and conclusions.

2 Methodology

2.1 Inversion method

CarbonTracker is an inverse modeling system developed by Peters et al. (2007). Optimized surface CO_2 fluxes with a 1°×1° horizontal resolution are calculated as follows:

$$F(x,y,t) = \lambda_r \cdot F_{bio}(x,y,t) + \lambda_r \cdot F_{ocn}(x,y,t) + F_{ff}(x,y,t) + F_{fire}(x,y,t), \quad (1)$$

where $F_{bio}(x,y,t)$, $F_{ocn}(x,y,t)$, $F_{ff}(x,y,t)$, and $F_{fire}(x,y,t)$ are the emissions from the biosphere, the ocean, fossil fuel, and fires. λ_r is the scaling factor to be optimized in the data assimilation process, corresponding to 156 ecoregions around the globe (126 land and 30 ocean regions). In the land, the ecoregions are defined as following the Transcom regions (Gurney et al., 2002) with ecosystem classification defined Olson et al. (1992). In the ocean, 30 ocean regions are defined following Jacobson et al. (2007). The scaling factor spans 5 weeks with 1 week resolution. In each assimilation cycle, the entire scaling factor is updated by 1 week observations by a time stepping approach. The assimilation window moves forward by 1 week at each assimilation cycle. After 5 assimilation cycles, the first part of the scaling factor analyzed by 5 weeks observations is regarded as the optimized scaling factor.

The EnKF data assimilation method used in CarbonTracker is the ensemble square root filter (EnSRF) suggested by Whitaker and Hamill (2002). The analysis equation for data assimilation is expressed as

$$\mathrm{x}^{\mathrm{a}} = \mathbf{K}\mathrm{y}^{\mathrm{o}} + (\mathbf{I}_n - \mathbf{KH})\mathrm{x}_{\mathrm{b}}, \quad (2)$$

where x^{a} is the n-dimensional analysis (posterior) state vector ; y^{o} is the p-dimensional observation vector (atmospheric CO_2 observations); $\mathbf{K}$ is the n × p dimensional Kalman gain; $\mathbf{I}_n$ is the identity matrix; $\mathbf{H}$ is the linearized observation operator, which transforms the information in the model space to the information in the observation space; and x^{b} is the background state vector. In CarbonTracker, the state vector corresponds to the scaling factor. The Kalman gain $\mathbf{K}$ is defined as

Atmos. Chem. Phys. Discuss., doi:10.5194/acp-2015-875, 2016
Manuscript under review for journal Atmos. Chem. Phys.
Published: 22 February 2016

Atmospheric Chemistry and Physics Discussions
Open Access
EGU

$$\mathbf{K} = \left(\mathbf{P}^{\mathrm{b}}\mathbf{H}^{\mathrm{T}}\right)\left(\mathbf{H}\mathbf{P}^{\mathrm{b}}\mathbf{H}^{\mathrm{T}} + \mathbf{R}\right)^{-1}, \tag{3}$$

where $\mathbf{P}^{\mathrm{b}}$ is the background error covariance; $\mathbf{R}$ is the observation error covariance or model data mismatch, which is predefined at each observation site. $\mathbf{P}^{\mathrm{b}}\mathbf{H}^{\mathrm{T}}$ and $\mathbf{H}\mathbf{P}^{\mathrm{b}}\mathbf{H}^{\mathrm{T}}$ in Eq. (3) can be calculated as

$$\mathbf{P}\mathbf{H}^{\mathrm{T}} \approx \frac{1}{m-1}\left(\mathrm{x}_1', \mathrm{x}_2', \ldots, \mathrm{x}_m'\right)\cdot\left(\mathbf{H}\mathrm{x}_1', \mathbf{H}\mathrm{x}_2', \ldots, \mathbf{H}\mathrm{x}_m'\right)^{\mathrm{T}}, \tag{4}$$

$$\mathbf{H}\mathbf{P}\mathbf{H}^{\mathrm{T}} \approx \frac{1}{m-1}\left(\mathbf{H}\mathrm{x}_1', \mathbf{H}\mathrm{x}_2', \ldots, \mathbf{H}\mathrm{x}_m'\right)\cdot\left(\mathbf{H}\mathrm{x}_1', \mathbf{H}\mathrm{x}_2', \ldots, \mathbf{H}\mathrm{x}_m'\right)^{\mathrm{T}}, \tag{5}$$

where m is the number of ensembles and $'$ denotes the perturbation of ensemble mean.

To reduce the sampling error and filter divergence due to the underestimation of background error covariance in the EnKF, the covariance localization method is used (Houtekamer and Mitchell, 2001). The localization is not applied to Marine Boundary Layer (MBL) sites (e.g. observation sites in Antarctica), because the MBL sites are considered as including information on large footprints of flux signals (Peters et al., 2007). The physical distance between the scaling factors cannot be defined. Therefore, localization is performed based on the linear correlation coefficient between the ensemble of the scaling factor and the ensemble of the model CO_2 concentration (Peters et al., 2007). The Kalman gain with an insignificant statistical value is set to zero after a statistical significance test, 95% significance level in a student's T-test, is performed on the correlations.

2.2 A priori flux data

Four types of a priori and imposed CO_2 fluxes used in this study are as follows: (1) First guess biosphere flux from the Carnegie–Ames–Stanford Approach Global Fire Emissions Database (CASA GFED) version 3.1 (van der Werf et al., 2010). The 3 hour interval Net Ecosytem Exchange (NEE) is calculated from monthly mean Net Primary Production (NPP) and ecosystem respiration (RE) by using a simple temperature Q_{10}[1] relationship and a linear

[1] It is calculated as $Q_{10}\left(t\right) = 1.5^{\left(\left(T_{2m} - T_0\right)/10.0\right)}$, where t is time, T_{2m} is temperature (K) at 2 m, and T_0 is 273.15 K.

Atmos. Chem. Phys. Discuss., doi:10.5194/acp-2015-875, 2016
Manuscript under review for journal Atmos. Chem. Phys.
Published: 22 February 2016

Atmospheric Chemistry and Physics Discussions

scaling of photosynthesis with solar radiation (Olsen and Randerson, 2004); (2) the prior ocean flux from air-sea partial pressure differences based on Jacobson et al. (2007). Short-term flux variability is derived from the atmospheric model wind speeds via the gas transfer coefficient; (3) biomass burning emissions obtained from GFED v3.1 (van der Werf et al., 2010); (4) the prescribed fossil fuel emission from the Carbon Dioxide Information and Analysis Center (CDIAC) and the Emission Database for Global Atmospheric Research (EDGAR) databases

2.3 Atmospheric CO_2 observations

Atmospheric CO_2 mole fraction observations measured at surface observation sites are used in this study. Figure 1 shows the observation network and Table 1 presents observation site information for the Asian and European regions. Three sets of atmospheric CO_2 observations data are assimilated: (1) surface CO_2 observations distributed by the NOAA ESRL (observation sites operated by NOAA, Environment Canada (EC), the Australian Commonwealth Scientific and Industrial Research Organization (CSIRO), the National Center for Atmospheric Research (NCAR), and Lawrence Berkeley National Laboratory (LBNL)); (2) World Data Centre for Greenhouse Gases (WDCGG, http://ds.data.jma.go.jp/wdcgg/); (3) JR-STATION observation data over Siberia operated by CGER/NIES (Sasakawa et al., 2010; 2013). The JR-STATION sites consist of nine towers (eight towers in west Siberia and one tower in east Siberia). At the BRZ (Berezorechka) site, in West Siberia, a light aircraft measures the vertical profiles of CO_2 from the PBL to the lower free troposphere (LFT). Atmospheric air was sampled at four levels on the BRZ tower and at two levels on the other eight towers. Sampled CO_2 data were calibrated against the NIES 09 CO_2 scale which are lower than the WMO-X2007 CO_2 scale by 0.07 ppm at around 360 ppm and consistent in the range between 380 and 400 ppm (Machida et al., 2011). Detailed description of JR-STATION sites can be found in Sasakawa et al. (2010; 2013). Daytime averaged CO_2 concentrations (1200-1600 LST, representing the time when active vertical mixing occurred in the PBL) for each day from the time series at the highest level of tower measurements are used in the data assimilation.

In CarbonTracker, model data mismatch (MDM) is determined by requiring innovation χ^2 statistics in Eq. (6) become one at each observation site (Peters et al. 2007).

Atmos. Chem. Phys. Discuss., doi:10.5194/acp-2015-875, 2016
Manuscript under review for journal Atmos. Chem. Phys.
Published: 22 February 2016

$$\chi^2 = \frac{(y^o - \mathbf{H}x^b)^2}{\mathbf{H}\mathbf{P}^b\mathbf{H}^T + \mathbf{R}}, \qquad (6)$$

The site categories and model-data mismatch values are assigned the same value as in previous studies (Peters et al., 2007; Kim et al. 2014b; Zhang et al., 2014b). For the JR-STATION sites, the model-data mismatch is set to 3 ppm, which is the same as for tower measurements in North America. The location of each observation site is represented in Fig. 1.

2.4 Experimental framework

Two experiments with different set of observations are conducted in this study: one experiment, the CNTL experiment, is conducted by using set of observations without observations in the Siberia region (black color observation sites represented in Fig. 1); the other experiment, the JR experiment, is conducted by using all available observations including the Siberia data (all observation sites represented in Fig. 1). The TM5 model (Krol et al., 2005) which calculates four-dimensional CO_2 concentration field runs at global 3°×2° horizontal resolution and a nesting domain centered in Asia with 1°×1° horizontal resolution. The nesting domain is shown in Fig. 1. Meteorological variables for running the TM5 transport model are from the European Centre for Medium-Range Weather Forecasts (ECMWF) forecast model output. The experimental period is from 1 January 2000 to 31 December 2009. The observation data commonly used for CNTL and JR experiments exists from 2000, but the additional Siberia data for the JR experiment exist from 2002. The number of ensembles is 150, and the scaling factor includes 5 weeks of lag, as in previous studies (Peters et al., 2007; Peters et al., 2010; Peylin et al., 2013; Kim et al., 2012, 2014a, 2014b; Zhang et al., 2014a, 2014b).

3 Results

3.1 Characteristics of carbon fluxes

In this section, optimized surface CO_2 fluxes inferred from two experiments are examined. The optimized surface CO_2 flux in 2000 and 2001 is excluded from this analysis because 2000 is considered a spin-up year similar to previous studies using CarbonTracker and JR-STATION data are used since 2002. Only the biosphere and ocean fluxes are presented here because fires (biomass burning) and fossil fuel emissions are not optimized in CarbonTracker.

Atmos. Chem. Phys. Discuss., doi:10.5194/acp-2015-875, 2016
Manuscript under review for journal Atmos. Chem. Phys.
Published: 22 February 2016

Atmospheric Chemistry and Physics
Open Access
Discussions

Figure 2 presents the spatial distribution of the averaged prior and optimized biosphere and ocean fluxes of the two experiments and the difference between the CNTL and JR experiments from 2002 to 2009. The optimized biosphere flux uptakes of the CNTL and JR experiments are greater than the prior flux uptakes (Figs. 2a, c, d). The differences in fluxes between the CNTL and JR experiments are distinctive in EB (Siberia) where the new additional observations are assimilated (Fig. 2b). The magnitude of surface CO_2 uptakes decreases in that region by assimilating JR-STATION observation data. On the contrary, the average surface CO_2 uptakes in other regions, such as North America, Europe, the western North Pacific Ocean, and the Atlantic Ocean, increase by assimilating JR-STATION observation data.

The difference in the optimized CO_2 flux between the two experiments is analyzed. Table 2 presents prior and optimized fluxes with their uncertainties for global total, global land, global ocean, and TransCom regions in the NH. Flux uncertainty is calculated as one-sigma standard deviation of the fluxes estimated, assuming Gaussian errors. The global total optimized CO_2 fluxes are similar for each experiment at -5.69±1.84 Pg C yr^{-1} (CNTL experiment) and -5.60±1.72 Pg C yr^{-1} (JR experiment), compared with the global prior flux of -3.94±2.23 Pg C yr^{-1}. The global land sink in the CNTL experiment is larger by 0.07 Pg C yr^{-1} than that of the JR experiment, and the global ocean sink in the CNTL experiment is smaller by 0.08 Pg C yr^{-1} than that of the JR experiment. The additional observations do not make any discrepancy between two the experiments with respect to the global total sink, and they indicate only a small difference in the land-ocean CO_2 flux partitioning. The estimated CO_2 flux uncertainty in the land region from the JR experiment is smaller than that of the CNTL experiment because new observations provide additional constraints on the optimized CO_2 flux. For specific regions in the NH, a large difference of optimized surface CO_2 flux is observed in the EB. The surface CO_2 uptakes in the EB of the CNTL experiment is -1.17±0.93 Pg C yr^{-1} and that of the JR experiment is -0.78±0.70 Pg C yr^{-1}, respectively. The uncertainty of the optimized surface CO_2 uptake in the EB from the JR experiment is reduced by assimilating additional observations. On the other hand, the surface CO_2 uptake increases in other regions of the NH.

Figure 3 presents the spatial distribution of the optimized biosphere fluxes difference between the CNTL and JR experiments from 2002 to 2009. The difference of optimized surface CO_2 flux is calculated as in Fig. 2b. The largest difference of optimized surface CO_2 fluxes between the two experiments occurs in Siberia. The uptake of optimized surface CO_2 flux in this region is reduced all years except 2003. In 2003, extreme drought occurred in the northern mid-latitudes (Knorr et al., 2007) and Europe (Ciais et al., 2005), which resulted in increased NEE (i.e. reduced uptake of CO_2). Despite the number of observations used in the optimization in 2003 being relatively smaller than that in the later experiment period, new observations in the JR experiment provide information on the reduced uptake of optimized surface CO_2 fluxes in 2003 in Siberia.

Optimized surface CO_2 fluxes averaged from 2002 to 2009 for each ecoregion in the NH are shown in Table 3. In the EB, optimized surface CO_2 uptake from the JR experiment is smaller (larger) than that of the CNTL experiment in the Conifer Forest and Northern Taiga (in other ecoregions). In the ET, Europe, North American Boreal (NAB), and North American Temperate (NAT) regions, the optimized surface CO_2 uptakes from the JR experiment are larger than those of the CNTL experiment in most ecoregions.

Figure 4 shows the histogram of annual and average optimized surface CO_2 fluxes over global total, global land, and global ocean. As shown in Table 2, the differences between annual and average optimized surface CO_2 fluxes over the globe are small and the average is almost the same for the two experiments (Fig. 4a), and the differences in global land and ocean are also small (Figs. 4b, c). The optimized surface CO_2 fluxes from each experiment show similar interannual variability, which implies that the additional Siberian observations do not affect the interannual variability of global surface CO_2 uptakes.

Figure 5 is the same as Fig. 4 but covers land regions in the NH. Although the optimized surface CO_2 fluxes over global total are similar, those over each TransCom region are different in each experiment. The difference between the two experiments is largest in the EB as expected (Fig. 5a). The JR experiment exhibits a weaker surface CO_2 uptake in the EB than does the CNTL experiment except for 2003 as shown in Fig. 3b, whereas the JR experiment exhibits a greater surface CO_2 uptake in the other regions, especially over Europe in 2008 and 2009, than the CNTL experiment (Figs. 5b, c, d, and e).

Figure 6 shows monthly optimized surface CO_2 fluxes averaged from 2002 to 2009 with their uncertainties from both experiments. The largest difference in surface CO_2 flux between the two experiments occurs in June and July, which represent the active season of the terrestrial ecosystem with a large surface CO_2 flux uncertainty. The JR experiment exhibits a weaker surface CO_2 summer uptake in the EB (Fig. 6a) and slightly greater uptake in the other

Atmos. Chem. Phys. Discuss., doi:10.5194/acp-2015-875, 2016
Manuscript under review for journal Atmos. Chem. Phys.
Published: 22 February 2016

Atmospheric Chemistry and Physics
Discussions

regions (Figs. 6b, c, d, and e). Additional Siberian data provides information on the surface CO_2 uptake by vegetation activity in the NH summer.

3.2 Comparison with observations

Table 4 presents the average bias of the model CO_2 concentrations calculated by the background and optimized fluxes of the two experiments at each observation site located in Asia and Europe from 2002 to 2009. The bias is calculated by subtracting the observed CO_2 concentrations from the model CO_2 concentrations. Biases of the JR experiment are smaller than those of the CNTL experiment at the JR-STATION sites, which indicates that the optimized surface CO_2 flux of the JR experiment is more consistent with the observed CO_2 concentrations than that in the CNTL experiment. The negative bias at five JR-STATION sites (DEM, IGR, KRZ, NOY, and YAK) located in the forest area of the EB is reduced compared with those of the CNTL experiment, which indicates that the optimized surface CO_2 uptake of the CNTL experiment is overestimated with respect to CO_2 concentration observations in Siberia. Otherwise, the reduced surface CO_2 uptake of the JR experiment exhibits more consistent model CO_2 concentrations in this region. Model CO_2 concentrations calculated by background surface CO_2 fluxes from the JR experiment are also more consistent with the observations, implying that background scaling factors of the JR experiment are more accurate than those of the CNTL experiment. In addition, the average innovation χ^2-statistics at the JR-STATION sites are generally close to 1, implying that the defined MDM is an appropriate value. Therefore, by assimilating JR-STATION observation data, the JR experiments exhibits better results than the CNTL experiment at observation sites in EB.

However, at observation sites in ET and Europe, the difference in biases of the two experiments is relatively small and not significant enough to determine which experiment exhibits better results. This is due to the small difference of optimized surface CO_2 fluxes between the two experiments in the ET region. The observation sites in Europe are located far from Eastern Europe and Siberia as shown in Fig. 1 so that they are not sensitive to the change of surface CO_2 uptake in those regions. In addition, the MDM at four sites (BAL, BSC, HUN, and OBN) in Europe is assigned as 7.5 ppm, the largest value in CarbonTracker, due to poor representation of the transport model at these sites.

Atmos. Chem. Phys. Discuss., doi:10.5194/acp-2015-875, 2016
Manuscript under review for journal Atmos. Chem. Phys.
Published: 22 February 2016

3.3 Effect of additional observations

The effects of additional observations on the optimized surface CO_2 flux are investigated. Figure 7 shows the average, maximum, average in summer (June, July, and August) and average in winter (December, January, February) uncertainty reductions from 2002 to 2009. The uncertainty reduction is calculated as follows:

$$\mathrm{UR} = \frac{\sigma_{CNTL} - \sigma_{JR}}{\sigma_{CNTL}} \times 100(\%) , \qquad (7)$$

where σ_{CNTL} and σ_{JR} are one-sigma standard deviations of the optimized scaling factor for CNTL experiment and JR experiment, respectively, assuming Gaussian errors. The maximum uncertainty reduction is the greatest value in any week in the period 2002 to 2009 in each ecoregion. As expected, the average uncertainty reduction is readily apparent in the Confer Forest of EB, which has additional observations (Fig. 7a). The uncertainty reduction of Asia and Europe, especially in the forest of Siberia and Eastern Europe, is greater than for other regions. The spatial pattern of the maximum uncertainty reduction is similar to that of the average values, but the magnitude of the maximum uncertainty reduction is higher than the average value, which implies that additional observations sometimes have a great impact on the optimization of surface CO_2 flux (Fig. 7b). The uncertainty reduction of EB in summer is higher than that in winter (Figs. 7c, d). For example, the average value of the Conifer Forest of EB is 29.1%, the maximum value is 78.6%, the average value in summer is 36.3% and the average value in winter is 29.7%, respectively. The result shows that the uncertainties of the optimized surface CO_2 fluxes are reduced by the additional observations.

To investigate the impact of individual observations, the self-sensitivities are calculated by the method demonstrated by Kim et al. (2014b). The self-sensitivity is the diagonal element of the influence matrix which measures the impact of individual observations in the observation space on the optimized surface CO_2 flux. Figure 8 shows the self-sensitivities of the two experiments averaged from 2002 to 2009. The average self-sensitivities at the JR-STATION sites are as large as those at the tower measurements in North America, i.e., Continuous site category observations in Fig. 1. The global average self-sensitivities are 4.83% (CNTL experiment) and 5.08% (JR experiment), and the cumulative impacts for the 5 weeks assimilation window are 18.79% (CNTL experiment) and 19.33% (JR experiment). The average self-sensitivities of additional observations are higher than those of other sites, providing much information for estimating surface CO_2 fluxes.

To assess the observation impact on the optimized surface CO_2 fluxes, the root mean square differences (RMSDs) between the optimized surface CO_2 fluxes and the background fluxes at each assimilation step in summer are calculated (Fig. 9). The RMSD of the analyzed surface CO_2 fluxes constrained by one week of observations from the background fluxes in JR experiment is greater than that in CNTL experiment (Figs. 9a, b). The RMSD values in Siberia are as high as those in North America, implying that surface CO_2 fluxes in Siberia are analyzed by direct observations at the first cycle. This is consistent with the high value of self-sensitivities at JR-STATION sites as shown in Fig. 8b. Kim et al. (2014b) showed that the RMSD in Asia increases after 5 weeks of optimization, which implies that it takes 5 weeks to affect the surface CO_2 fluxes in Siberia by the transport of the CO_2 concentrations observed in remote regions. However, by assimilating the CO_2 concentrations observed at the JR-STATION sites in Siberia, the observation impact on the optimized surface CO_2 fluxes in Siberia increases after 1 week of optimization (Fig. 9b).

On the other hands, the RMSD in the Siberia region increases after 5 weeks of optimization in the CNTL experiment compared to that in the JR experiment (Figs. 9c, d), which corresponds to the reduced uptake of optimized surface CO_2 fluxes in JR experiment as shown in Fig. 2b.

3.4 Comparison with other results

A comparison of the optimized surface CO_2 flux in this study with other inversion studies is presented in Table 5. In the EB, the land sink from the JR experiment (-0.78±0.70 Pg C yr^{-1}) is smaller than those reported by Zhang et al. (2014b) (-1.02 Pg C yr^{-1}), Maki et al. (2010) (-1.46±0.41 Pg C yr^{-1}), and the CT2013B results (-1.09±4.03 Pg C yr^{-1}), but higher than those reported by Saeki et al. (2013) (-0.35±0.41 Pg C yr^{-1}; including biomass burning 0.11 Pg C yr^{-1}). Because CT2013B and Zhang et al. (2014b) use the same inversion framework as this study, the reduced land sink is caused by assimilating additional observations. The difference in land sink between the JR experiment and Saeki et al. (2013) is caused by a different inversion system framework.

In Europe, though the long-term average land sink from the JR experiment (-0.35±0.65 Pg C yr^{-1}) is similar to that of CTE2014 (-0.33±0.80 Pg C yr^{-1}), the average land sink from 2008-2009 of the JR experiment (-0.75±0.63 Pg C yr^{-1}) is much higher than that of CTE2014 (-0.11±0.38 Pg C yr^{-1}). According to Reuter et al. (2014), despite the different experiment period, the land sink of Europe in 2010 (-1.02±0.30 Pg C yr^{-1}) estimated by using satellite

Atmos. Chem. Phys. Discuss., doi:10.5194/acp-2015-875, 2016
Manuscript under review for journal Atmos. Chem. Phys.
Published: 22 February 2016

Atmospheric Chemistry and Physics Discussions

observations is much higher than previous inversion studies (e.g., Peylin et al. 2013) using only surface observations. The land sinks of the JR experiment in 2008 and 2009 are -0.67 and -0.75 Pg C yr^{-1}, respectively, whereas much lower uptakes (-0.21, -0.39 Pg C yr^{-1}) are obtained for the CNTL experiment. Overall, the optimized surface CO_2 fluxes of JR experiment are comparable to those of other previous studies.

4 Summary and conclusions

In this study, to investigate the effect of the Siberian observations, which are not used in the previous studies using CarbonTracker, on the optimization of surface CO_2 fluxes, two experiments, named CNTL and JR, with different sets of observations from 2000 to 2009 were conducted and optimized surface CO_2 fluxes from 2002 to 2009 were analyzed.

The global balances of the sources and sinks of surface CO_2 fluxes were maintained for both experiments, while the distribution of the optimized surface CO_2 fluxes changed. The magnitude of the optimized biosphere surface CO_2 uptake in EB (Siberia) was decreased, whereas it was increased in other regions of the NH (Eurasian Temperate, Europe, North American Boreal, and North American Temperate). The land sink of Europe increased significantly for 2008 and 2009, which is consistent with the other inversion results inferred by satellite observations. Additional observations are used to correct the surface CO_2 uptake in June and July, the active vegetation uptake season, in terms of monthly average optimized surface CO_2 fluxes. As a result, the additional observations do not exhibit a change in the magnitude of the global surface CO_2 flux balance because they provide detailed information about the Siberian land sink instead of the global land sink magnitude, when they are used in the well-constructed inversion modeling system.

The model CO_2 concentration using the background and optimized surface CO_2 fluxes in the JR experiment are more consistent with the CO_2 observations than those in the CNTL experiment, showing lower biases in the EB region. On the other hand, the differences of biases in ET and Europe between the two experiments are not distinguishable.

The new observations provide useful information on the optimized surface CO_2 fluxes. The observation impact of the Siberian observation data is investigated by means of uncertainty reduction and self-sensitivity calculated by an influence matrix. Additional observations reduce the uncertainty of the optimized surface CO_2 fluxes in Asia and Europe, mainly in the

EB (Siberia), where the new observations are used in the assimilation. The average self-sensitivities of the JR-STATION sites are as large as other continuous measurements (e.g., tower measurements in North America). The global average self-sensitivity and cumulative impact of the JR experiment are higher than that of the CNTL experiment, which implies that the individual observation impact of JR-STATION data on optimized surface CO_2 fluxes is higher than the average values. The RMSD of the analyzed surface CO_2 fluxes constrained by one week of observations from the background fluxes also suggests that new Siberian observations provide a larger amount of information on the optimized surface CO_2 fluxes.

This study reaffirms that the JR-STATION data affect the longitudinal distribution of the total NH sinks, especially in the EB and Europe, when it is used by atmospheric CO_2 inversion modeling. In the future, it is expected that Siberian observations will be used as an important constraint for estimating surface CO_2 fluxes over the NH with various CO_2 observations (e.g. satellite and aircraft measurements) simultaneously.

Acknowledgements

This study was funded by the Korea Meteorological Administration Research and Development Program under the Grant KMIPA 2015-2021 .and by the Yonsei University Yonsei-SNU Collaborative Research Fund of 2015. The JR-STATION is supported by the Global Environment Research Account for National Institutes of the Ministry of the Environment, Japan and the Russian Foundation for Basic Research (Grant No. 14-05-00590).

Atmos. Chem. Phys. Discuss., doi:10.5194/acp-2015-875, 2016
Manuscript under review for journal Atmos. Chem. Phys.
Published: 22 February 2016

References

Bruhwiler, L. M. P., Michalak, A. M., and Tans, P. P.: Spatial and temporal resolution of carbon flux estimates for 1983-2002, Biogeosciences, 8, 1309-1331, doi:10.5194/bg-8-1309-2011, 2011.

Chevallier, F., Bréon, F.-M., and Rayner, P. J.: Contribution of the Orbiting Carbon Observatory to the estimation of CO_2 sources and sinks: Theoretical study in a variational data assimilation framework, J. Geophys. Res. Atmos., 112, D09307, doi:10.1029/2006JD007375, 2007

Chevallier, F., Ciais, P., Conway, T. J., Aalto, T., Anderson, B. E., Bousquet, P., Brunke, E. G., Ciattaglia, L., Esaki, Y., Fröhlich, M., Gomez, A., Gomez-Pelaez, A. J., Haszpra, L., Krummel, P. B., Langenfelds, R. L., Leuenberger, M., Machida, T., Maignan, F., Matsueda, H., Morguí, J. A., Mukai, H., Nakazawa, T., Peylin, P., Ramonet, M., Rivier, L., Sawa, Y., Schmdit, M., Steele, L. P., Vay, S. A., Vermeulen, A. T., Wofsy, S., and Worthy, D.: CO_2 surface fluxes at grid point scale estimated from a global 21 year reanalysis of atmospheric measurements, J. Geophys. Res. Atmos., 115, D21307, doi 10.1029/2010jd013887, 2010

Ciais, P., Reichstein, M., Viovy, N., Granier, A., Ogee, J., Allard, V., Aubinet, M., Buchmann, N., Bernhofer, C., Carrara, A., Chevallier, F., De Noblet, N., Friend, A. D., Friedlingstein, P., Grunwald, T., Heinesch, B., Keronen, P., Knohl, A., Krinner, G., Loustau, D., Manca, G., Matteucci, G., Miglietta, F., Ourcival, J. M., Papale, D., Pilegaard, K., Rambal, S., Seufert, G., Soussana, J. F., Sanz, M. J., Schulze, E. D., Vesala, T., and Valentini, R.: Europe-wide reduction in primary productivity caused by the heat and drought in 2003, Nature, 437, 529–533, 2005.

Feng, L., Palmer, P. I., Parker, R. J., Deutscher, N. M., Feist, D. G., Kivi, R., Morino, I. and Sussmann, R.: Elevated uptake of CO_2 over Europe inferred from GOSAT XCO2 retrievals: a real phenomenon or an artefact of the analysis?, *Atmos. Chem. Phys. Discuss.*, **15**, 1989-2011, doi:10.5194/acpd-15-1989-2015, 2015.

Gurney, K. R., Law, R. M., Denning, A. S., Rayner, P. J., Baker, D., Bousquet, P., Bruhwiler, L., Chen, Y. H., Ciais, P., Fan, S., Fung, I. Y., Gloor, M., Heimann, M., Higuchi, K., John, J., Maki, T., Maksyutov, S., Masarie, K., Peylin, P., Prather, M., Pak, B. C., Randerson, J., Sarmiento, J., Taguchi, S., Takahashi, T., and Yuen, C. W.: Towards robust regional estimates of CO_2 sources and sinks using atmospheric transport models, Nature, 415, 626–630, 2002.

Hayes, D. J., McGuire, A. D., Kicklighter, D. W., Gurney, K. R., Burnside, T. J., and Melillo, J. M.: Is the northern high-latitude land-based CO_2 sink weakening?, Global Biogeochem. Cy., 25, GB3018, doi:10.1029/2010GB003813, 2011.

Houghton, R. A., Butman, D., Bunn, A. G., Krankina, O. N., Schlesinger, P., and Stone, T. A.: Mapping Russian forest biomass with data from satellites and forest inventories. Environ. Res. Lett., 2, 045032, doi:10.1088/1748-9326/2/4/045032, 2007.

Houtekamer, P. L., and Mitchell, H. L.: A sequential ensemble Kalman filter for atmospheric data assimilation, Mon. Wea. Rev., 129, 123-137, 2001.

Jacobson, A. R., Mikaloff Fletcher, S. E., Gruber, N., Sarmiento, J. L., and Gloor, M.: A joint atmosphere–ocean inversion for surface fluxes of carbon dioxide: 1. Methods and global-scale fluxes, Global Biogeochem. Cy., 21, B1019, doi:10.1029/2005GB002556, 2007.

Kim, J., Kim, H. M., and Cho, C.-H.: Application of Carbon Tracking System based on ensemble Kalman Filter on the diagnosis of Carbon Cycle in Asia, Atmosphere, 22(4), 415-447, 2012. (in Korean with English abstract)

Kim, J., Kim, H. M., and Cho, C.-H.: The effect of optimization and the nesting domain on carbon flux analyses in Asia using a carbon tracking system based on the ensemble Kalman filter, Asia-Pacific J. Atmos. Sci., 50, 327-344, doi:10.1007/s13143-014-0020-7, 2014a.

Kim, J., H. M. Kim, and C.-H. Cho, 2014b: Influence of CO_2 observations on the optimized CO_2 flux in an ensemble Kalman filter, Atmos. Chem. Phys., 14, 13515-13530, doi:10.5194/acp-14-13515-2014, 2014b.

Knorr, W., Gobron, N., Scholze, M., Kaminski, T., Schnur, R., and Pinty, B.: Impact of terrestrial biosphere carbon exchanges on the anomalous CO_2 increase in 2002-2003, Geophys. Res. Lett., 34, L09703, doi:10.1029/2006GL029019, 2007.

Krol, M., Houweling, S., Bregman, B., Broek, M., van der Segers, A., Velthoven, P. V., Peters, W., Dentener, F., and Bergamaschi, P.: The two-way nested global chemistry-transport zoom model TM5: Algorithm and applications, Atmos. Chem. Phys., 5, 417-432, 2005.

Kurganova, I. N., Kudeyarov, V. N., and Lopes De Gerenyu, V. O.: Updated estimate of carbon balance on Russian territory, Tellus, 62B, 497-505, doi:10.1111/j.1600-0889.2010.00467.x, 2010.

Le Quéré, C., Moriarty, R., Andrew, R. M., Peters, G. P., Ciais, P., Friedlingstein, P., Jones, S. D., Sitch, S., Tans, P., Arneth, A., Boden, T. A., Bopp, L., Bozec, Y., Canadell, J. G., Chini, L. P., Chevallier, F., Cosca, C. E., Harris, I., Hoppema, M., Houghton, R. A., House, J. I., Jain, A. K., Johannessen, T., Kato, E., Keeling, R. F., Kitidis, V., Klein Goldewijk, K., Koven, C., Landa, C. S., Landschützer, P., Lenton, A., Lima, I. D., Marland, G., Mathis, J. T., Metzl, N., Nojiri, Y., Olsen, A., Ono, T., Peng, S., Peters, W., Pfeil, B., Poulter, B., Raupach, M. R., Regnier, P., Rö- denbeck, C., Saito, S., Salisbury, J. E., Schuster, U., Schwinger, J., Séférian, R., Segschneider, J., Steinhoff, T., Stocker, B. D., Sutton, A. J., Takahashi, T., Tilbrook, B., van der Werf, G. R., Viovy, N., Wang, Y.-P., Wanninkhof, R., Wiltshire, A., and Zeng, N.: Global carbon budget 2014, Earth Syst. Sci. Data, 7, 47–85, doi:10.5194/essd-7-47-2015, 2015.

Lloyd, J., Langenfelds, R. L., Francey, R. J., Gloor, M., Tchebakova, N. M., Zolotoukhine, D., Brand, W. A., Werner, R. A., Jordan, A., Allison, C. A., Zrazhewske, V., Shibistova, O., and Schulze, E.-D.: A trace-gas climatology above Zotino, central Siberia, Tellus, 54B, 749-767, 2002.

Machida, T., Matsueda, H., Sawa, Y., Nakagawa, Y., Hirotani, K., Kondo, N., Goto, K., Nakazawa, T., Ishikawa, K., and Ogawa, T.: Worldwide Measurements of Atmospheric CO_2 and Other Trace Gas Species Using Commercial Airlines, J. Atmos. Oceanic Techno., 25, 1744-1754, doi:10.1175/2008JTECHA1082.1, 2008.

Machida, T., Tohjima, Y., Katsumata, K., and Mukai, H.: A new CO_2 calibration scale based on gravimetric one-step dilution cylinders in National Institute for Environmental Studies-NIES 09 CO_2 scale, GaW Report, 194, 114-119, *15th WMO/IAEA Meeting of Experts on Carbon Dioxide, Other Greenhouse Gases and Related Tracers Measurement Techniques*, WMO/TM No. 1553, 2011.

Maki, T., Ikegami, M., Fujita, T., Hirahara, T., Yamada, K., Mori, K., Takeuchi, A., Tsutsumi, Y., Suda, K., and Conway, T. J.: New technique to analyse global distributions of CO_2 concentrations and fluxes from non-processed observational data, Tellus, 62B, 797-809, doi:10.1111/j.1600-0889.2010.00488.x, 2010.

Maksyutov, S., Machida, T., Mukai, H., Patra, P. K., Nakazawa, T., Inoue, G., and Transcom-3 Modelers: Effect of recent observations on Asia CO_2 flux estimates by transport model inversions, Tellus, 55B, 522-529, 2003.

Miller, C. E., Crisp, D., DeCola, P. L., Olsen, S. C., Randerson, J. T., Michalak, A. M., Alkhaled, A., Rayner, P., Jacob, D. J., Suntharalingam, P., Jones, D. B. A., Denning, A. S., Nicholls, M. E., Doney, S. C., Pawson, S., Boesch, H., Connor, B. J., Fung, I. Y., O'Brien, D. O., Salawitch, R. J., Sander, S. P., Sen, B., Tans, P., Toon, G. C., Wennberg, P. O., Wofsy, S. C., Yung, Y. L., and Law, R. M.: Precision requirements for space-based XCO_2 data, J. Geophys. Res., 112, D10314, doi:10.1029/2006JD007659, 2007.

Olson, J., Watts, J., and Allsion, L.: Major World Ecosystem Complexes Ranked by Carbon in Live Vegetation: a Database, Tech. rep., Carbon Dioxide Information Analysis Center, U.S. Department of Energy, Oak Ridge National Laboratory, Oak Ridge, Tennessee, USA, doi:10.3334/CDIAC/lue.ndp017, 1992.

Paris, J.-D., Ciais, P., Nédélec, P., Ramonet, M., Belan, B. D., Arshinov, M. Y., Golitsyn, G. S., Granberg, I., Stohl, A., Cayez, G., Athier, G., Boumard, F., and Cousin, J. M.: The YAK-AEROSIB transcontinental aircraft campaigns: new insights on the transport of CO_2, CO and O_3 across Siberia, Tellus B, 60, 551– 568, 2008.

Peters, W., Jacobson, A. R., Sweeney, C., Andrews, A. E., Conway, T. J., Masarie, K., Miller, J. B., Bruhwiler, L. M. P., Petron, G., Hirsch, A. I., Worthy, D. E. J., van der Werf, G. R., Randerson, J. T., Wennberg, P. O., Krol, M. C., Tans, P. P.: An atmospheric perspective on North American carbon dioxide exchange: CarbonTracker, Proc. Nat. Acd. Sci. U.S.A., 104, 18925-18930, 2007.

Peters, W., Krol, M. C., van der Werf, G. R., Houweling, S., Jones, C. D., Hughes, J., Schaefer, K., Masarie, K. A., Jacobson, A. R. Miller, J. B., Cho, C. H., Ramonet, M., Schmidt, M., Ciattaglia, L., Apadula, F., Heltai, D., Meinhardt, F., di Sarra, A. G., Piacentino, S., Sferlazzo, D., Aalto, T., Hatakka, J., Ström, J., Haszpra, L., Meijer, H. A. J., van der Laan, S., Neubert, R. E. M., Jordan, A., Rodó, X., Morguí, J. A., Vermeulen, A. T., Popa, E., Rozanski, K., Zimnoch, M., Manning, A. C., Leuenberger, M., Uglietti, C., Dolman, A. J., Ciais, P. Heimann, M., and Tans, P. P.: Seven years of recent European net terrestrial carbon dioxide exchange constrained by atmospheric observations, Global Change Biol., 16, 1317-1337, doi:10.1111/j.1365-2486.2009.02078.x, 2010.

Peylin P., Law, R. M., Gurney, K. R., Chevallier, F., Jacobson A. R., Maki, T., Niwa, Y., Patra, P. K., Peters, W., Rayner, P. J., Rödenbeck, C., van der Laan-Luijkx, I. T., and Zhang, X.: Global atmospheric carbon budget: results from an ensemble of atmospheric CO_2 inversions, Biogeosciences, 10, 6699-6720, doi:10.5194/bg-10-6699-2013, 2013.

Olsen, S. C., and Randerson, J. T.: Differences between surface and column atmospheric CO_2 and implications for carbon cycle research, J. Geophys. Res., 109, D02301, doi:10.1029/2003JD003968, 2004.

Quegan, S., Beer, C., Shvidenko, A., McCallum, I., Handoh, I. C., Peylin, P., Rödenbeck, C., Lucht, W., Nilsson, S., and Schmullius, C.: Estimating the carbon balance of central Siberia using landscape-ecosystem approach, atmospheric inversion and dynamic global vegetation models, Glob. Change Biol., 17, 351-365, doi:10.1111/j.1365-2486.2010.02275.x, 2011.

Reuter, M., Buchwitz, M., Hilker, M., Heymann, J., Schneising, O., Pillai, D., Bovensmann, H., Burrows, J. P., Bösch, H., Parker, R., Butz, A., Hasekamp, O., O'Dell, C. W., Yoshida, Y., Gerbig, C., Nehrkorn, T., Deutscher, N. M., Warneke, T., Notholt, J., Hase, F., Kivi, R., Sussmann, R., Machida, T., Matsueda, H., and Sawa, Y.: Satellite-inferred European carbon sink larger than expected, Atmos. Chem. Phys., 14, 13739-13753, doi:10.5194/acp-14-13739-2014, 2014.

Saeki, T., Maksyutov, S., Sasakawa, M., Machida, T., Arshinov, M., Tans, P. P., Conway, T. J., Saito, M., Valsala, V., Oda, T., Andres, R. J., and Belikov, D.: Carbon flux estimation for Siberia by inverse modeling constrained by aircraft and tower CO_2 measurements, J. Geophys. Res. Atmos., 118, 1100-1122, doi:10.1002/jgrd.50127, 2013.

Sasakawa, M., Shimoyama, K., Machida, T., Tsuda, N., Suto, H., Arshinov, M., Davydov, D., Fofonov, A., Krasnov, O., Saeki, T., Koyama, Y., and Maksyutov, S.: Continuous measurements of methane from a tower network over Siberia, Tellus, 62B, 403-416, doi:10.1111/j.1600-0889.2010.00494.x, 2010.

Sasakawa, M., Machida, T., Tsuda, N., Arshinov, M., Davydov, D., Fofonov, A., and Krasnov, O.: Aircraft and tower measurements of CO_2 concentration in the planetary boundary layer and the lower free troposphere over southern taiga in West Siberia: Long-term records from 2002 to 2011, J. Geophys. Res. Atmos., 118, 9489-9498, doi:10.1002/jgrd.50755, 2013.

Atmos. Chem. Phys. Discuss., doi:10.5194/acp-2015-875, 2016
Manuscript under review for journal Atmos. Chem. Phys.
Published: 22 February 2016

Schepaschenko, D., McCallum, I., Shvidenko, A., Fritz, S., Kraxner, F., and Obersteiner, M, : A new hybrid land cover dataset for Russia: a methodology for integrating statistics, remote sensing and in situ information, J. Land Use Sci., 6, 245-259, doi:10.1080/1747423X.2010.511681, 2011.

Schneising, O., Buchwitz, M., Reuter, M., Heymann, J., Bovensmann, H., and Burrows, J. P.: Long-term analysis of carbon dioxide and methane column-averaged mole fractions retrieved from SCIAMACHY, Atmos. Chem. Phys., 11, 2863-2880, doi:10.5194/acp-11-2863-2011, 2011

Schulze, E.-D., Lloyd, J., Kelliher, F. M., Wirth, C., Rebmann, C., Lühker, B., Mund, M., Knohl, A., Milyukova, I. M., Schulze, W., Ziegler, W., Varlagin, A. B., Sogachev, A. F., Valentini, R., Dore, S., Grigoriev, S., Kolle, O., Panfyorov, M. I., Tchebakova, N., and Vygodskaya, N. N.: Productivity of forests in the Eurosiberian boreal region and their potential to act as a carbon sink – a synthesis. Glob. Change Biol., 5, 703-722, doi:10.1046/j.1365-2486.1999.00266.x, 1999.

Tarnocai, C., Canadell, J. G., Schuur, E. A. G., Kuhry, P., Mazhitova, G., and Zimov, S.: Soil organic carbon pools in the northern circumpolar permafrost region, Glob. Biogeochem. Cycles, 23, GB2023, doi:10.1029/2008GB003327, 2009.

Turnbull, J. C., Miller, J. B., Lehman, S. J., Hurst, D., Peters, W., Tans, P. P., Southon, J., Montzka, S. A., Elkins, J. W., Mondeel, D. J., Romashkin, P. A., Elansky, N., and Skorokhod, A.: Spatial distribution of $\Delta^{14}CO_2$ across Eurasia: measurements from the TROICA-8 expedition, Atmos. Chem. Phys., 9, 175-187, doi:10.5194/acp-9-175-2009, 2009.

van der Werf, G. R., Randerson, J. T., Giglio, L., Collatz, G. J., Mu, M., Kasibhatla, P. S., Morton, D. C., DeFries, R. S., Jin, Y., and van Leeuwen, T. T.: Global fire emissions and the contribution of deforestation, savanna, forest, agricultural, and peat fires (1997–2009), Atmos. Chem. Phys., 10, 11707–11735, doi:10.5194/acp-10-11707-2010, 2010.

Whitaker, J. S., and Hamill, T. M.: Ensemble Data Assimilation without Perturbed Observations, Mon. Wea. Rev., 130, 1913-1924, 2002.

Winderlich, J., Chen, H., Gerbig, C., Seifert, T., Kolle, O., Lavrič,, Kaier, C., Höfer, A., and Heimann, H.: Continuous low-maintenance CO_2/CH_4/H_2O measurements at the Zotino Tall Tower Observatory (ZOTTO) in Central Siberia, Atmos. Meas. Tech., 3, 1113-1128, doi:10.5194/amt-3-1113-2010, 2010.

Zhang, H. F., Chen, B. Z., van der Laan-Luijkx, I. T., Chen, J., Xu, G., Yan, J. W., Zhou, L. X., Fukuyama, Y., Tans, P. P., and Peters, W.: Net terrestrial CO_2 exchange over China during 2001–2010 estimated with an ensemble data assimilation system for atmospheric CO_2. J. Geophys. Res. Atmos., 119, 2013JD021297, doi:10.1002/2013JD021297, 2014a.

Zhang, H. F, Chen, B. Z., van der Laan-Luijkx, Machida, T., Matsueda, H., Sawa, Y, Fukuyama, Y., Labuschange, C., Langenfelds, R., van der Schoot, M., Xu, G., Yan, J. W., Zhou, L. X., Tans, P. P., and Peters, W.: Estimating Asian terrestrial carbon fluxes from CONTRAIL aircraft and surface CO_2 observations for the period 2006 to 2010, Atmos. Chem. Phys., 14, 5807-5824, doi:10.5194/acp-14-7807-2014, 2014b.

Atmos. Chem. Phys. Discuss., doi:10.5194/acp-2015-875, 2016
Manuscript under review for journal Atmos. Chem. Phys.
Published: 22 February 2016

Table 1. Information on observation sites located in the Asia and Europe region. MDM represents the model-data mismatch which is the observation error.

Site	Location	Latitude	Longitude	Height (m)	Laboratory	MDM (ppm)
AZV	Azovo, Russia	54.71°N	73.03°E	110	NIES	3
BRZ	Berezorechka, Russia	56.15°N	84.33°E	168	NIES	3
DEM	Demyanskoe, Russia	59.79°N	70.87°E	63	NIES	3
IGR	Igrim, Russia	63.19°N	64.41°E	9	NIES	3
KRS	Karasevoe, Russia	58.25°N	82.42°E	76	NIES	3
NOY	Noyabrsk, Russia	63.43°N	75.78°E	108	NIES	3
SVV	Savvushka, Russia	51.33°N	82.13°E	495	NIES	3
VGN	Vaganovo, Russia	54.50°N	62.32°E	192	NIES	3
YAK	Yakutsk, Russia	62.09°N	129.36°E	264	NIES	3
WLG	Mt. Waliguan, China	36.29°N	100.9°E	3810	CMA/ESRL	1.5
BKT	Bukit Kototabang, Indonesia	0.20°S	100.312°E	864	ESRL	7.5
WIS	Sede Boker, Israelr,	31.13°N	34.88°E	400	ESRL	2.5
KZD	Sary Taukum, Kazakhstan	44.45°N	77.57°E	412	ESRL	2.5
KZM	Plateau Assy, Kazakhstan	43.25°N	77.88°E	2519	ESRL	2.5
TAP	Tae-ahn Peninsula, South Korea	36.73°N	126.13°E	20	ESRL	5
UUM	Ulaan Uul, Mongolia	44.45°N	111.10°E	914	ESRL	2.5
CRI	Cape Rama, India	15.08°N	73.83°E	60	CSIRO	3
LLN	Lulin, Taiwan	23.47°N	120.87°E	2862	ESRL	7.5
SDZ	Shangdianzi, China	40.39°N	117.07°E	287	CMA/ESRL	3
MNM	Minamitorishima, Japan	24.29°N	153.98°E	8	JMA	3
RYO	Ryori, Japan	39.03°N	141.82°E	260	JMA	3
YON	Yonagunijima, Japan	24.47°N	123.02°E	30	JMA	3
GSN	Gosan, South Korea	33.15°N	126.12°E	72	NIER	3
BAL	Baltic Sea, Poland	55.35°N	17.22°E	3	ESRL	7.5
BSC	Black Sea, Constanta, Romania	44.17°N	28.68°E	3	ESRL	7.5
HUN	Hegyhatsal, Hungary	46.95°N	16.65°E	248	ESRL	7.5
OBN	Obninsk, Russia	55.11°N	36.60°E	183	ESRL	7.5
OXK	Ochsenkopf, Germany	50.03°N	11.80°E	1022	ESRL	2,5
PAL	Pallas-Sammaltunturi, GaW Station, Finland	67.97°N	24.12°E	560	ESRL	2.5
STM	Ocean Station M, Norway	66.00°N	2.00°E	0	ESRL	1.5

Atmos. Chem. Phys. Discuss., doi:10.5194/acp-2015-875, 2016
Manuscript under review for journal Atmos. Chem. Phys.
Published: 22 February 2016

Atmospheric Chemistry and Physics Discussions

Table 2. A prior and optimized surface CO_2 fluxes and their one-sigma uncertainties (Pg C yr^{-1} Region^{-1}) of global total, land, and ocean averaged spatially from 2002 to 2009.

Region	A priori	CNTL	JR.
Eurasian Boreal	-0.07±1.10	-1.17±0.93	-0.77±0.70
Eurasian Temperate	-0.05±0.49	-0.32±0.41	-0.37±0.40
Europe	-0.02±-0.76	-0.22±0.67	-0.38±0.64
North American Boreal	-0.04±0.61	-0.30±0.38	-0.36±0.38
North American Temperate	-0.03±0.66	-0.56±0.41	-0.60±0.41
Global total	-3.94±2.23	-5.59±1.84	-5.60±1.72
Global land	-1.36±1.90	-3.64±1.57	-3.57±1.43
Global ocean	-2.58±1.18	-1.95±0.97	-2.03±0.96

Table 3. The optimized surface CO_2 fluxes (Pg C yr^{-1} $Region^{-1}$) of ecosystem types at Eurasian Boreal, Eurasian Temperate, Europe, North American Boreal, and North American Temperate region averaged over 2002 - 2009.

Ecosystem type	Eurasian Boreal		Eurasian Temperate		Europe		North American Boreal		North American Temperate	
	CNTL	JR	CNTL	JR	CNTL	JR	CNTL	JR	CNTL	JR
Conifer Forest	-0.816	-0.338	-0.005	-0.005	-0.068	-0.071	-0.107	-0.121	-0.055	-0.070
Broadleaf Forest	-0.006	-0.014	-0.004	-0.005	-0.005	-0.005	0.000	0.000	-0.002	-0.002
Mixed Forest	-0.050	-0.090	-0.030	-0.035	-0.026	-0.063	-0.053	-0.054	-0.020	-0.021
Grass/Shrub	-0.035	-0.056	-0.248	-0.287	-0.017	-0.032	0.000	-0.001	-0.077	-0.081
Tropical Forest	0.000	0.000	-0.001	-0.001	0.000	0.000	0.000	0.000	0.000	0.000
Scrub/Woods	0.000	0.000	-0.002	-0.002	-0.001	-0.001	0.000	0.000	-0.013	-0.013
Semitundra	-0.146	-0.189	-0.008	-0.010	-0.008	-0.009	-0.057	-0.087	-0.010	-0.011
Fields/Woods/Savanna	-0.013	-0.022	-0.005	-0.006	0.003	-0.010	-0.004	-0.004	-0.149	-0.154
Northern Taiga	-0.094	-0.030	0.000	0.000	-0.006	-0.007	-0.066	-0.078	0.000	0.000
Forest/Field	-0.003	-0.008	0.006	0.005	-0.087	-0.106	-0.001	-0.001	-0.013	-0.017
Wetland	-0.002	-0.014	0.000	-0.000	-0.001	-0.002	-0.003	-0.006	-0.002	-0.003
Shrub/Tree/Suc	0.000	0.000	-0.001	-0.001	0.000	0.000	0.000	0.000	0.000	0.000
Crops	-0.002	-0.008	-0.019	-0.022	-0.011	-0.078	0.000	0.000	-0.216	-0.227
Wooded tundra	-0.003	-0.005	0.000	0.000	0.003	0.003	-0.003	-0.003	0.000	0.000
Water	0.000	0.000	-0.000	-0.000	-0.001	-0.001	-0.001	-0.001	-0.001	-0.001

Atmos. Chem. Phys. Discuss., doi:10.5194/acp-2015-875, 2016
Manuscript under review for journal Atmos. Chem. Phys.
Published: 22 February 2016

Table 4. Average differences between: model CO_2 concentrations (ppm) simulated using the background and the observed CO_2 concentration (ppm) (fourth and sixth columns), model CO_2 concentrations (ppm) simulated using the optimized surface CO_2 flux and the observed CO_2 concentration (ppm) (fifth and seventh columns), and average innovation χ^2 from 2002 to 2009 at observation sites located in Asia and Europe (eighth column).

Region	Site	MDM [ppm]	CNTL		JR		
			Bias (background)	Bias (optimized)	Bias (background)	Bias (optimized)	Innovation $\chi2$
Eurasian Boreal	AZV	3	1.68	1.04	0.77	0.19	0.85
	BRZ	3	1.41	0.68	0.67	0.39	1.17
	DEM	3	0.15	-0.84	0.32	0.11	0.84
	IGR	3	-1.58	-2.71	-0.52	-1.26	1.15
	KRS	3	0.57	-0.22	0.27	0.12	1.22
	NOY	3	-0.02	-1.06	0.16	0.00	0.86
	SVV	3	1.25	0.71	0.63	0.09	0.96
	VGN	3	2.55	2.11	1.50	0.84	1.18
	YAK	3	0.23	-2.18	0.87	0.03	1.36
Eurasian Temperate	WLG	1.5	0.17	0.19	0.15	0.16	1.09
	BKT	7.5	4.12	4.06	4.13	4.05	0.57
	WIS	2.5	0.27	0.12	0.22	0.07	0.72
	KZD	2.5	1.79	0.98	1.42	1.14	1.26
	KZM	2.5	1.17	0.96	1.13	0.93	1.26
	TAP	5	0.50	0.55	0.58	0.71	0.58
	UUM	2.5	0.24	-0.07	0.20	0.12	1.05
	CRI	3	-1.95	-1.57	-1.94	-1.56	0.66
	LLN	7.5	4.42	3.09	4.42	3.09	0.47
	SDZ	3	-3.02	-5.26	-3.09	-5.28	2.08
	MNM	3	0.56	0.52	0.59	0.56	0.17
	RYO	3	1.26	1.16	1.32	1.32	1.07
	YON	3	1.10	0.98	1.14	1.07	0.56
	GSN	3	-1.92	-1.71	-1.92	-1.70	1.83
Europe	BAL	7.5	-1.23	-1.32	-1.31	-1.45	0.37
	BSC	7.5	-4.12	-4.97	-4.12	-5.13	1.01
	HUN	7.5	0.93	0.53	0.86	0.36	0.46
	OBN	7.5	0.70	-0.71	0.59	-0.89	0.44
	OXK	2.5	0.50	0.02	0.43	-0.09	1.52
	PAL	2.5	0.47	0.07	0.58	0.16	0.76
	STM	1.5	0.54	0.42	0.55	0.42	0.76

Atmos. Chem. Phys. Discuss., doi:10.5194/acp-2015-875, 2016
Manuscript under review for journal Atmos. Chem. Phys.
Published: 22 February 2016

Atmospheric Chemistry and Physics Discussions
Open Access

Table 5. Optimized surface CO_2 fluxes (Pg C yr^{-1}) from this study and other inversion studies.

Citation	Area	Estimate surface CO_2 flux	Period	Remarks
This study	Eurasian Boreal	-0.77±0.70	2002-2009	JR experiment
Saeki et al. (2013)	Eurasian Boreal	-0.35±0.61	2000-2009	Including biomass burning (0.11Pg C yr-1), Using JR-STATION observations
Zhang et al. (2014b)	Eurasian Boreal	-1.02±0.91	2006-2010	Using CONTRAL observations
Maki et al. (2010)	Eurasian Boreal	-1.46±0.41	2001-2007	
CT2013B	Eurasian Boreal	-1.09±4.03	2001-2012	
This study	Europe	-0.38±0.64 -0.75±0.63	2002-2009 2008-2009	JR experiment
Reuter et al. (2014)	Europe	-1.02±0.30	2010	Using satellite data
CTE2014	Europe	-0.33±0.80 -0.11±0.38	2001-2013 2008-2009	

Atmos. Chem. Phys. Discuss., doi:10.5194/acp-2015-875, 2016
Manuscript under review for journal Atmos. Chem. Phys.
Published: 22 February 2016

Atmospheric Chemistry and Physics
Discussions

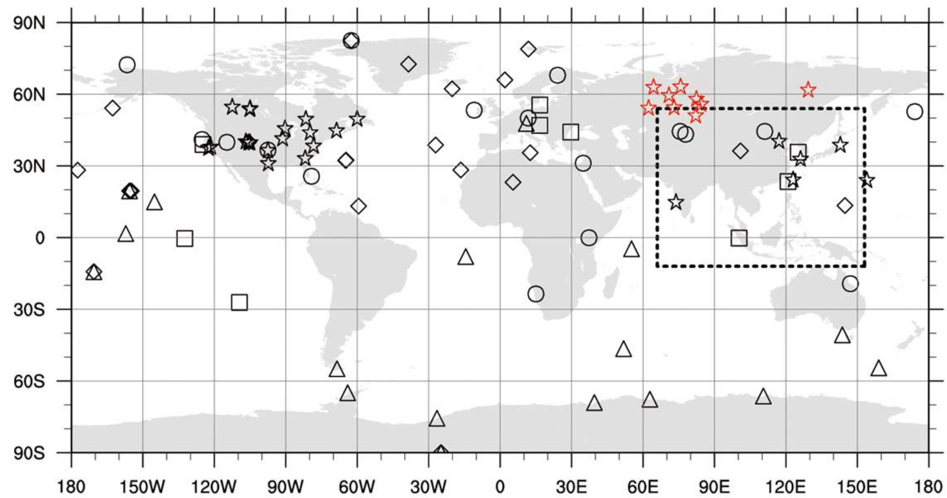

Figure 1. Observation networks of CO_2 concentrations around the globe and the nested domain of the TM5 transport model over Asia (dashed box). Each observation site is assigned to different categories (△ : MBL; ○: Continental; ◇: Mixed land/ocean and mountain; ☆: Continuous; □: Difficult). JR-STATION observation sites are represented in red color.

Atmos. Chem. Phys. Discuss., doi:10.5194/acp-2015-875, 2016
Manuscript under review for journal Atmos. Chem. Phys.
Published: 22 February 2016

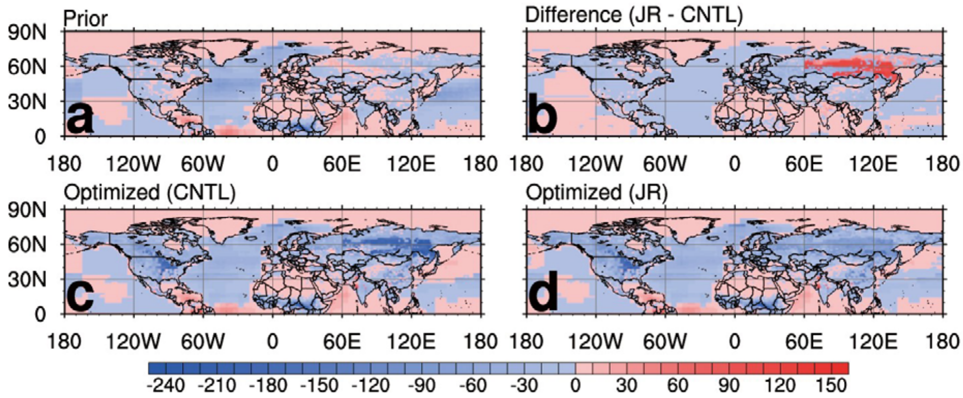

Figure 2. Average biosphere and ocean fluxes (gC m^{-2} yr^{-1}) from 2002 to 2009 of (a) the prior flux, (b) the difference between the optimized fluxes in the JR and CNTL experiments, (c) the optimized flux in the CNTL experiment, and (d) the optimized flux in the JR experiment. Blue colors (negative) denote net CO_2 flux uptake while red colors (positive) denote net CO_2 release to the atmosphere. The difference is calculated by subtracting surface CO_2 flux of CNTL experiment from that of JR experiment.

Atmos. Chem. Phys. Discuss., doi:10.5194/acp-2015-875, 2016
Manuscript under review for journal Atmos. Chem. Phys.
Published: 22 February 2016

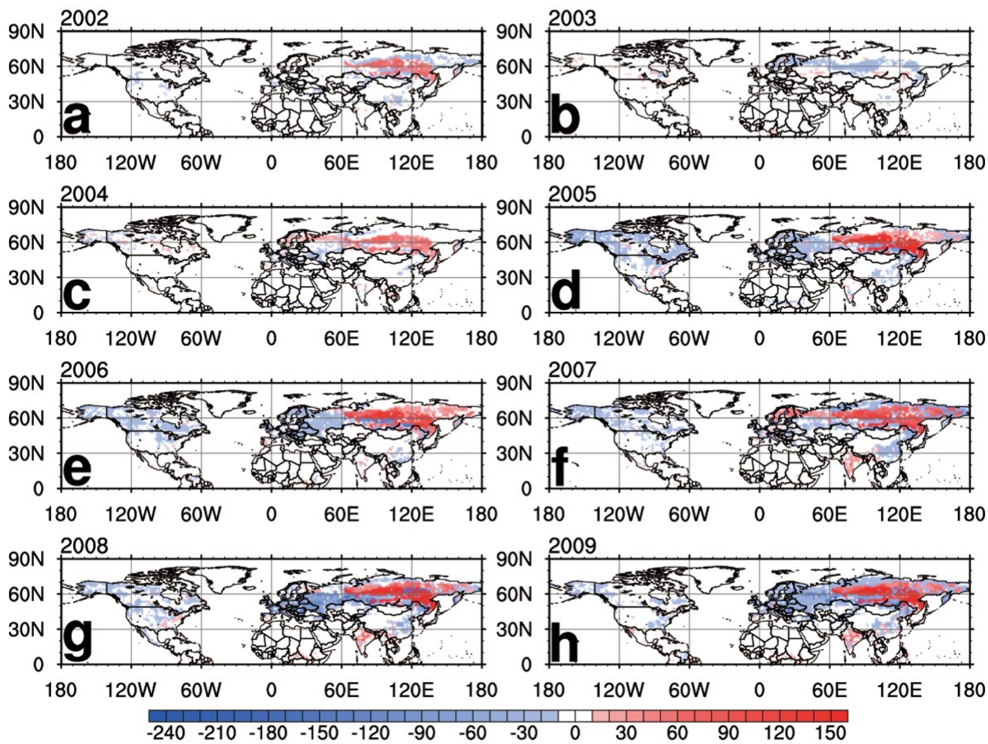

Figure 3. The difference between the optimized biosphere fluxes from the JR and CNTL experiment (g C m^{-2} yr^{-1}) of (a) 2002, (b) 2003, (c) 2004, (d) 2005, (e) 2006, (f) 2007, (g) 2008, and (h) 2009. Blue colors (negative) denote net CO_2 flux uptake while red colors (positive) denote net CO_2 release to the atmosphere. The difference is calculated by subtracting surface CO_2 flux of CNTL experiment from that of JR experiment.

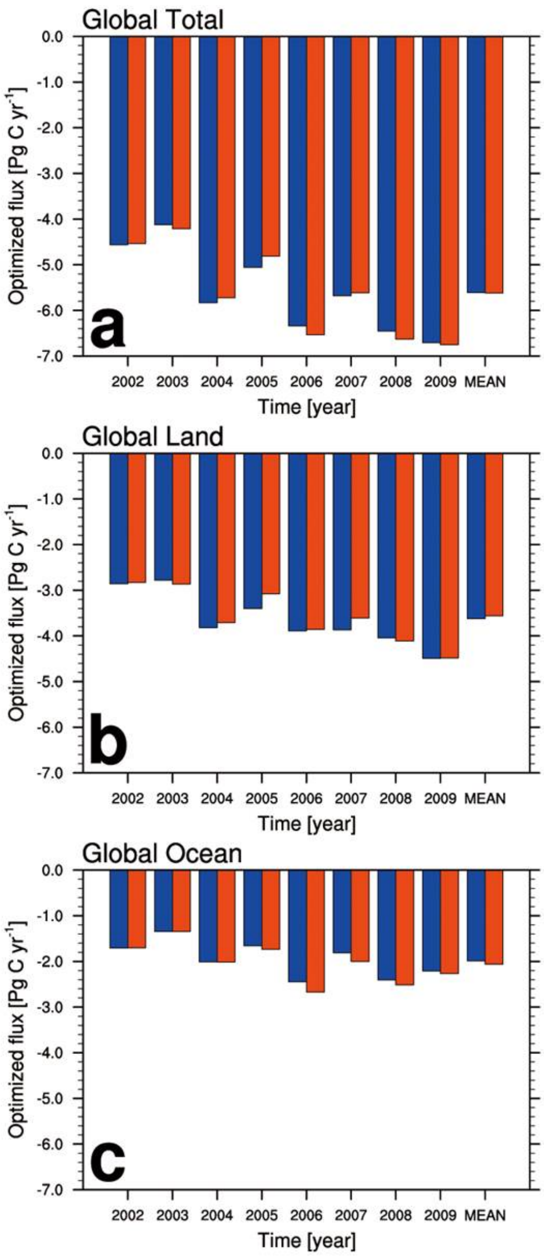

Figure 4. Annual and average biosphere and ocean fluxes (Pg C yr^{-1}) from the CNTL (blue bar) and JR (red bar) experiment aggregated over the (a) whole globe, (b) land, and (c) ocean.

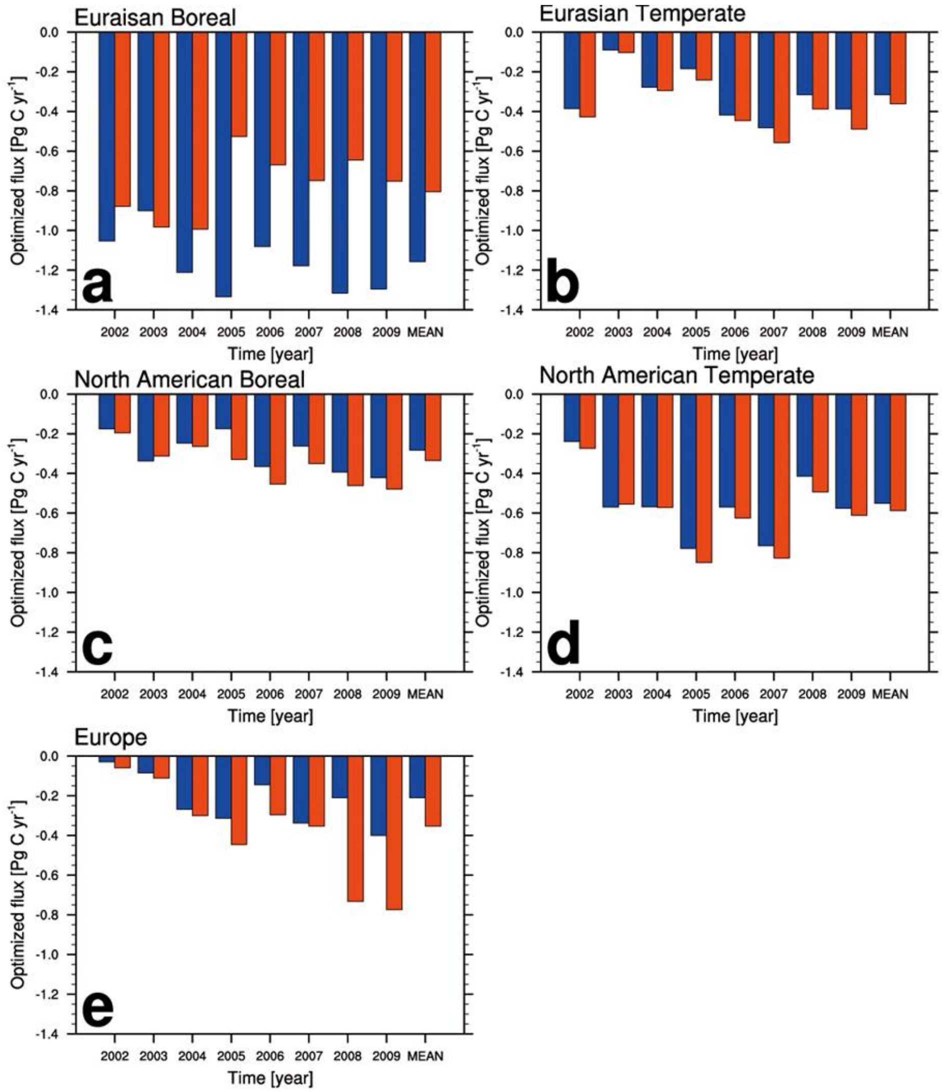

Figure 5. Annual and average biosphere and ocean fluxes (Pg C yr^{-1}) from the CNTL (blue bar) and JR (red bar) experiment aggregated over the (a) Eurasian Boreal, (b) Eurasia Temperate, (c) North American Boreal, (d) North American Temperate, and (e) Europe.

Atmos. Chem. Phys. Discuss., doi:10.5194/acp-2015-875, 2016
Manuscript under review for journal Atmos. Chem. Phys.
Published: 22 February 2016

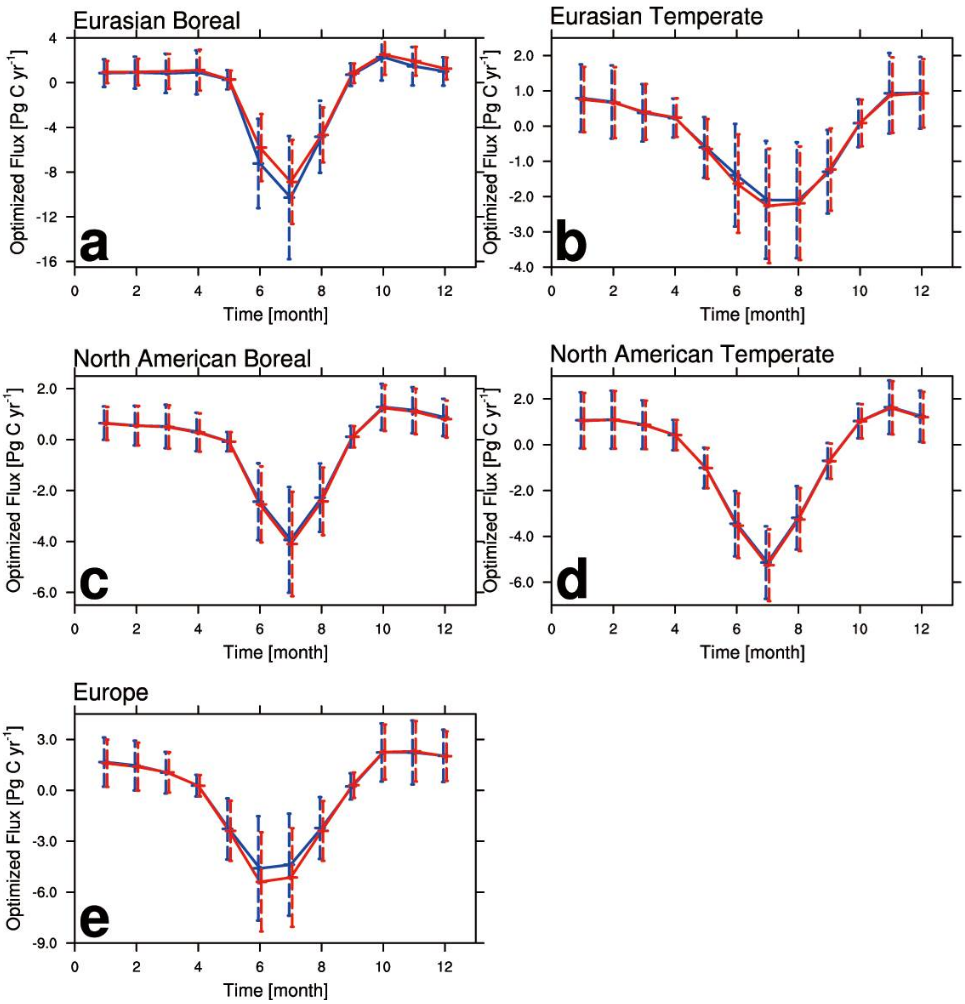

Figure 6. The monthly optimized biosphere fluxes averaged from 2002 to 2009 of CNTL (blue) and JR (red) experiment with their uncertainties over the (a) Eurasian Boreal, (b) Eurasian Temperate, (c) North American Boreal, (d) North American Temperate, and (e) Europe.

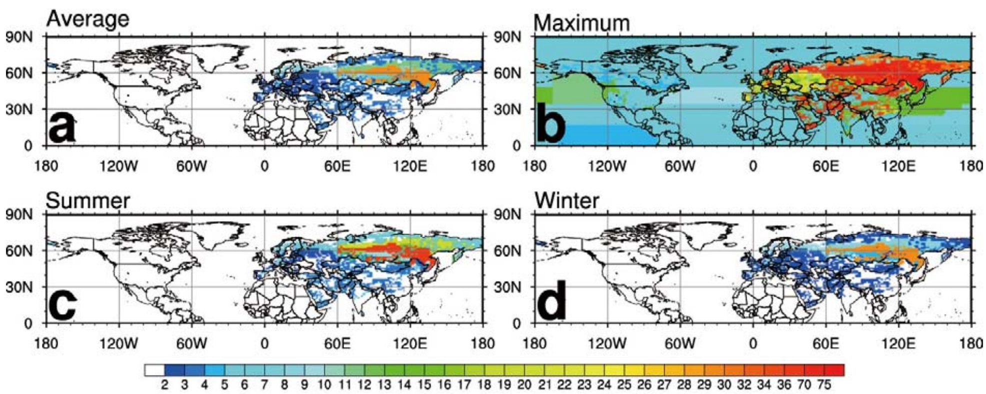

Figure 7. (a) Average uncertainty reduction (%) from 2002 to 2009, and (b) maximum uncertainty reduction (%) in any week from 2002 to 2009, average uncertainty reduction (%) in (c) summer, and (d) winter for the estimated uncertainty of the JR experiment relative to that of the CNTL experiment. Red (blue) denotes relatively high (low) value of uncertainty reduction.

Atmos. Chem. Phys. Discuss., doi:10.5194/acp-2015-875, 2016
Manuscript under review for journal Atmos. Chem. Phys.
Published: 22 February 2016

Atmospheric Chemistry and Physics
Discussions

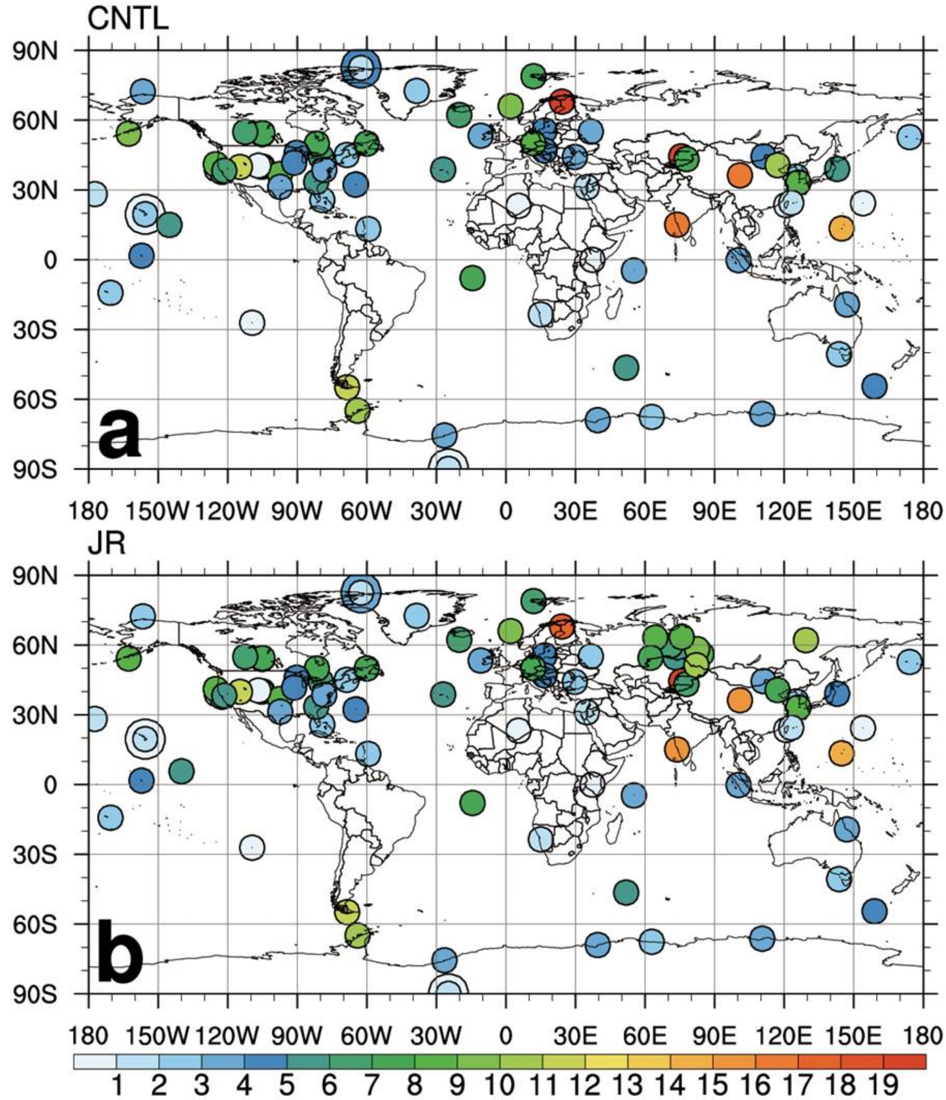

Figure 8. Self-sensitivity at each observation site averaged from 2002 to 2009 of (a) CNTL experiment and (b) JR experiment. The overlapping observation sites at the same locations or at close locations are distinguished by different sizes of circles. Red (blue) denotes relatively high (low) value of self-sensitivity.

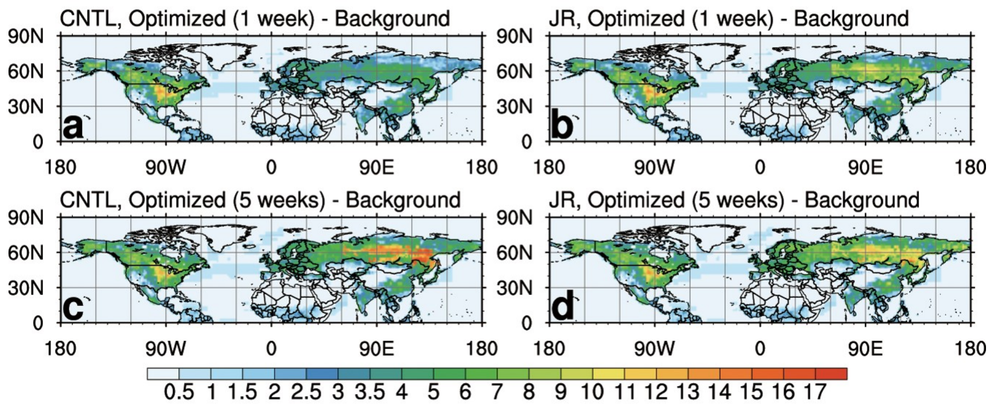

Figure 9. RMSD averaged from 2002 to 2009 between the background flux and posterior flux optimized by 1 week of observations in Northern Hemisphere summer of (a) CNTL experiment and (b) JR experiment; and RMSD averaged from 2002 to 2009 between the background flux and posterior flux optimized by 5 weeks of observations in Northern Hemisphere summer of (c) CNTL experiment and (d) JR experiment. The units are g C m^{-2} $week^{-1}$. Red (blue) denotes relatively high (low) value of RMSD.